

# Correlation Between Sub- $T_g$ Relaxation Processes and Mechanical Behavior for Different Hydrothermal Ageing Conditions in Epoxy Assemblies

M. Chevalier,<sup>1</sup> E. Dantras,<sup>1</sup> C. Tonon,<sup>2</sup> P. Guigue,<sup>3</sup> C. Lacabanne,<sup>1</sup> C. Puig,<sup>2</sup> C. Durin<sup>3</sup>

<sup>1</sup>Laboratoire de Physique des Polymères, Institut Carnot CIRIMAT, Université Paul Sabatier, Toulouse Cedex 31062, France

<sup>2</sup>Astrium, 31 avenue des Cosmonautes, Toulouse 31402, France

<sup>3</sup>Centre National d'Etudes Spatiales, 18 avenue Edouard Belin, Toulouse 31401, France

Received 22 January 2009; accepted 11 August 2009

DOI 10.1002/app.31253

Published online 15 September 2009 in Wiley InterScience (www.interscience.wiley.com).

**ABSTRACT:** The aim of this study is to understand aging phenomena by monitoring physical parameters after real and simulated aging experiments. This study focuses on aluminum-epoxy assemblies, which are commonly used on spacecraft structures. Different samples are submitted to simulated aging tests. Influence of temperature and moisture is analyzed. Evolution with aging is characterized at two different scales. The macroscopic behavior of the assemblies is studied by single lap shear test. A decrease in the shear rupture stress is observed with increasing temperature and relative humidity. It is demonstrated that temperature has more important influence. The molecular behavior in the adhesive joint is studied by dynamic dielectric spectroscopy measurements. This experiment gives access to molecular mobility in the adhesive. Dipolar entities are identified

as evolving with aging conditions. The temperature is more effective than moisture at this scale. An interpretation of the molecular mobility before and after aging shows that water is an important parameter of this study. A link between mechanical and molecular behavior with hydrothermal aging is found. The decrease of mechanical properties occurs while failures become interfacial. In the same time, the interactions between hydroxyether and water increase. The evolution of the macroscopic behavior of the bonded assemblies is due to this combination observed at different scales. © 2009 Wiley Periodicals, Inc. *J Appl Polym Sci* 115: 1208–1214, 2010

**Key words:** epoxy; adhesive; dielectric spectroscopy; aging; single lap shear

## INTRODUCTION

Aging processes in materials used for space applications depend on various parameters (on ground and space environments) and are not fully understood. The influence of each factor remains obscure. A particular attention shall be paid on the aging of bonded assemblies due to storage on ground and thermal cycling in orbit.

During spacecraft integration, in clean room, materials are used under humid and thermal controlled conditions:  $21 \pm 2^\circ\text{C}$ ,  $50 \pm 5\%\text{RH}$ . The integration activities and the storage can last several years. Consequently, it is necessary to take into account the time spent in clean room as an aging factor. An aging process, which begins before the launch could be the cause of an irreversible damage during the flight. All the structures of the satellite

are submitted to these controlled environmental conditions. The characterization and the simulation of aging phenomena in bonded assemblies are the challenge to improve their conception and their durability. Checking these assemblies after the launch is impossible. One alternative is to use accelerated testing on the basis of space industry knowledge and ESA normative data.<sup>1</sup> Empirical laws are the only way to obtain accelerated aging conditions. But, the link between accelerated testing and real-time aging is unknown. The aim of this study is to shed some light on this correlation.

The methodology used for the work presented later is to carry out an investigation of the mechanical behavior and molecular dynamics evolutions in thermoset bonded structures exposed to moisture. The combined use of mechanical and dielectric measurements has been chosen to evaluate epoxy-water interactions at macroscopic and molecular scales.

Epoxy-amine networks are relatively hydrophilic materials. They are able to absorb 1–6% per weight of water in many industrial formulations.<sup>2</sup> Numerous studies have been devoted to the water

Correspondence to: E. Dantras (dantras@cict.fr).

absorption process in these systems but this problem remains only partly understood.<sup>2–6</sup> Water ingress in polyepoxy networks leads to a range of effects<sup>3</sup>: bulk dissolution by water in the polymer network, moisture absorption on the surface of free volume holes in the glassy structure, interaction of water with hydrophilic polar moieties, such as amines and hydroxyls by strong hydrogen bonds. It is also reported that water is present in two different forms in polyepoxy networks<sup>4,7–9</sup>: free water that fills the microvoids of the network and bound water that bonds with polar groups.

A decrease in mechanical properties of bulk and bonded polyepoxy networks, such as modulus and rupture strength under humid conditions is observed. It is related to plasticization.<sup>9–11</sup> But how absorbed water affects the mobility of polymer chains is not well known. According to Mijovic et al.,<sup>5</sup> the chemical and physical changes on the molecular level during the early stage of environmental exposure is the most important point in the prediction of performance in adhesive joints.

The use of dynamic mechanical and dielectric measurements allows us to investigate the molecular dynamics. In polyepoxy systems, two to four relaxation regions have been reported by different experimental techniques.<sup>12–16</sup> Some authors studied the influence of water on molecular dynamics of amine cured epoxy adhesives.<sup>5,8,10,12</sup> They reported that some relaxational processes were influenced by the ingress of water into the network. But some results are contradictory, probably due to the complexity of the commercial adhesive formulations.

Therefore, the main objective of this study is to get a simultaneous evaluation of macroscopic and molecular changes in bonded structures exposed to hydrothermal environment.

## EXPERIMENTAL

### Materials

The studied system is an aluminum-epoxy assembly. The adhesive is a commercial amine-epoxy bicomponent adhesive packaged to be usable immediately. The two parts are prepared and a nozzle allows us to make and extrude the mix with an accurate repeatability. The hardener (part A) is a mix of several components, where aliphatic amine is preponderant. The part B is based on diglycidyl ether of bisphenol-A epoxy resin mixed with other components (fillers, catalyst...). Parts A and B are mixed at room temperature (ratio 2 : 1). The curing process is 7 days at  $21 \pm 2^\circ\text{C}$ ,  $50 \pm 5\% \text{RH}$ . It leads to two glassy transitions ( $T_g$ ) determined by Diathermal Scanning Calorimetry measurements. One, equal to

$60^\circ\text{C}$ , is associated with the high-crosslink network. The second one, equal to  $10^\circ\text{C}$ , corresponds to the low-crosslink regions. Both substrates are wrought aluminum alloys (2024 or 2017) widely used in aerospace industry. By this way, differential thermal expansions ( $\Delta\text{CTE}$ ) between the two substrates are avoided. This assembly is considered as a model. The joint thickness is ranging from 70 to 200  $\mu\text{m}$ .

### Hydrothermal aging conditions

During accelerated hydrothermal aging tests, the joints are exposed to a warm humid environment during 7 days. The temperature range is from 20 to  $80^\circ\text{C}$  (step =  $20^\circ\text{C}$ ) and the relative humidity is ranging from 20%RH to vapor saturation by steps of 20%RH. Each temperature–relative humidity pair is tested.

### Methods

#### Single lap shear test

Single lap shear tests are performed at  $25^\circ\text{C}$  using the tensile tension machine Instron 4505 with a 100 kN load cell. The crosshead speed is 1 mm/min. Three specimens were studied for each test. Data were recorded with the Serie IX software. The ruptures were analyzed visually to determine the percentage of cohesive failure.

#### Thermo mechanical analysis

Thermo mechanical measurements are performed using an Advanced Rheometric Expansion System strain controlled rheometer (TA Instruments) in the torsion rectangular mode within the linear elasticity range. Dynamic mechanical storage and loss modulus  $G'$  and  $G''$  were recorded as function of temperature from  $-50$  to  $100^\circ\text{C}$  at  $3^\circ\text{C}/\text{min}$ , for an angular frequency equal to 1 rad/s.

#### Dynamic dielectric spectroscopy

Broadband dielectric measurements are performed using a Novocontrol BDS 4000 covering a frequency range from  $10^{-2}$  Hz to  $10^6$  Hz with 10 points per decade. Experiments were carried out isothermally from  $-150$  to  $150^\circ\text{C}$  by steps of  $5^\circ\text{C}$ . The temperature is controlled with an accuracy of  $\pm 0.5^\circ\text{C}$  by a nitrogen gas stream heated by a Quatro temperature controller. The samples are round plate assemblies ( $\Phi = 40$  mm). We use the aluminum alloy substrates as electrodes.

The real  $\epsilon'$  and imaginary  $\epsilon''$  parts of the relative complex permittivity  $\epsilon^*$  are measured as a function of frequency  $f$  at a given temperature  $T$ . Experimental data are fitted by the Havriliak-Negami (HN)

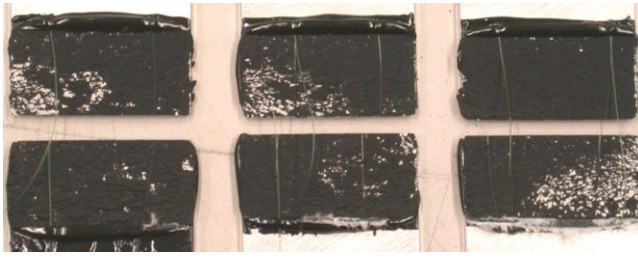


**Figure 1** Fracture appearance for three single lap shear samples at initial state. [Color figure can be viewed in the online issue, which is available at [www.interscience.wiley.com](http://www.interscience.wiley.com).]

[eq. (1)] function with an additional conductivity term.<sup>17,18</sup>

$$\varepsilon^*(\omega) = \varepsilon_{\infty} + \frac{(\varepsilon_s - \varepsilon_{\infty})}{(1 + (i\omega\tau_{\text{HN}})^{\alpha_{\text{HN}}})^{\beta_{\text{HN}}}} + \frac{\sigma_0}{i\varepsilon_0\omega} \quad (1)$$

where  $\varepsilon_{\infty}$  is the real permittivity for high frequencies,  $\Delta\varepsilon$  is the relaxation strength,  $\alpha_{\text{HN}}$  and  $\beta_{\text{HN}}$  are the HN parameters,  $\tau_{\text{HN}}$  is the relaxation time,  $\omega$  is the angular frequency,  $\sigma_0$  is the d.c. conductivity, and  $\varepsilon_0$  the dielectric permittivity of vacuum.

## RESULTS

### Mechanical behavior

#### Static mechanical behavior

The shear behavior is characterized at initial state. The shear rupture stress  $\sigma_R$  is  $27.5 \pm 0.3$  MPa. The fracture appearance is cohesive as shown in Figure 1. The cohesive surface is  $89 \pm 1\%$  of the bonded surface. These values are considered as reference values before aging.

Single lap shear tests are performed after different aging conditions. The shear rupture stresses are

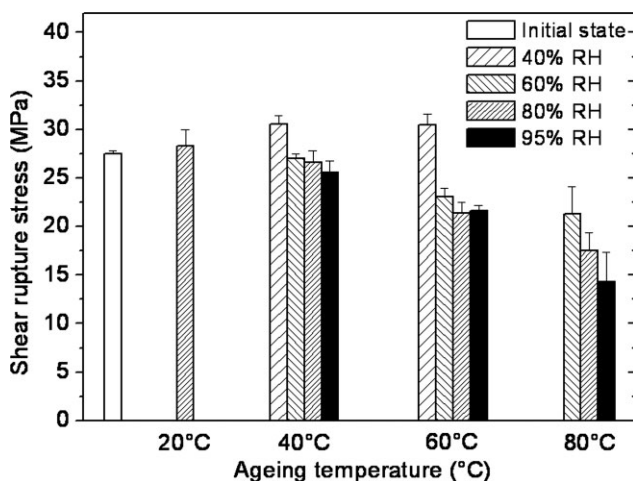


**Figure 2** Evolution of the shear rupture stress as a function of temperature and humidity percentage.

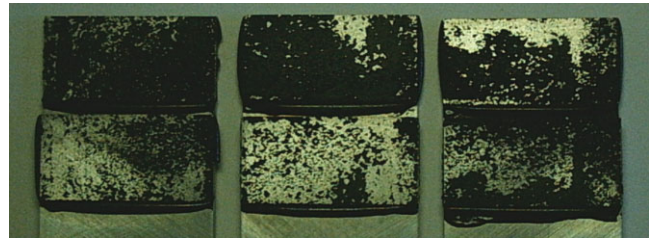


**Figure 3** Fracture appearance for three single lap shear samples after 7 days under  $80^\circ\text{C}$ , 95%RH. [Color figure can be viewed in the online issue, which is available at [www.interscience.wiley.com](http://www.interscience.wiley.com).]

shown in Figure 2 as function of aging temperature for different relative humidity percentage. First, we note that  $\sigma_R$  is higher than  $\sigma_R$  at initial state when the relative moisture percentage of the tests is 40%RH, i.e. lower than clean room conditions. For this moisture environment,  $\sigma_R$  value is independent of the aging temperature. For a given relative humidity percentage,  $\sigma_R$  exhibits a linear decrease as function of temperature. The influence of relative humidity is also analyzed. For isothermal aging conditions, a nonlinear decrease of  $\sigma_R$  is observed as function of moisture amount. The higher the temperature is, the higher the moisture influence.

The evolution of the failures is studied. Figure 3 shows the failure after aging at  $80^\circ\text{C}$ , 95%RH. The cohesive failure percentage is reported in the Table I. As function of increasing aging temperature and humidity, we note that the rupture becomes more interfacial. For  $80^\circ\text{C}$  and 95%RH aging conditions, we observe that the ratio between interfacial and cohesive failures is about one.

#### Dynamic mechanical behavior

The storage modulus  $G'$  and loss modulus  $G''$  are shown in Figure 4 as function of temperature for the bulk adhesive at initial state. The conservative modulus decreases from 1 GPa at  $-45$ – $0.8$  GPa at  $40^\circ\text{C}$ . From 50 to  $80^\circ\text{C}$ , the decrease is stronger.  $G'$  reaches 10 MPa. This transition is associated with the mechanical manifestation of glass transition. The loss modulus exhibits two relaxation phenomena

**TABLE I**  
Cohesive Failure Percentage as a Function of Hydrothermal Ageing Conditions

Aging moisture (%RH)	Aging temperature ( $^\circ\text{C}$ )			
	20	40	60	80
40	N/A	$87 \pm 4$	$78 \pm 3$	N/A
60	N/A	$77 \pm 11$	$65 \pm 12$	$79 \pm 9$
80	$80 \pm 2$	$75 \pm 6$	$60 \pm 4$	$61 \pm 7$
95	N/A	$70 \pm 11$	$61 \pm 1$	$45 \pm 7$



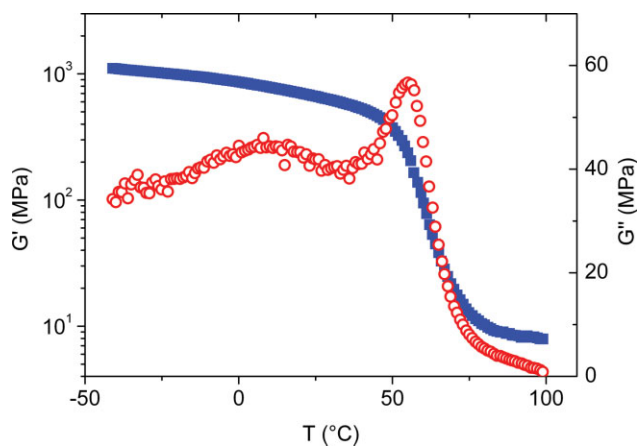


**Figure 4** Storage modulus  $G'$  (squares) and loss modulus  $G''$  (circles) as function of temperature for the bulk adhesive at initial state. [Color figure can be viewed in the online issue, which is available at [www.interscience.wiley.com](http://www.interscience.wiley.com).]

called  $\omega$  and  $\alpha$ .  $\omega$  peak reaches a maximum at 10°C. This relaxation is associated with heterogeneities in the adhesive.<sup>19</sup>  $\alpha$  reaches a maximum at  $T_\alpha$  temperature equal to 55°C.

### Dielectric behavior

#### Molecular mobility at initial state

The dielectric loss from -150 to 150°C of an assembly at initial state shown in Figure 5. Six dielectric phenomena are pointed out. In the low temperature range a weak and broad relaxation mode is observed, labeled  $\gamma$ . At higher temperature, a more intense and narrow atypical mode  $\beta_2$  is found. Then, a weak and broad mode is detected: this mode is

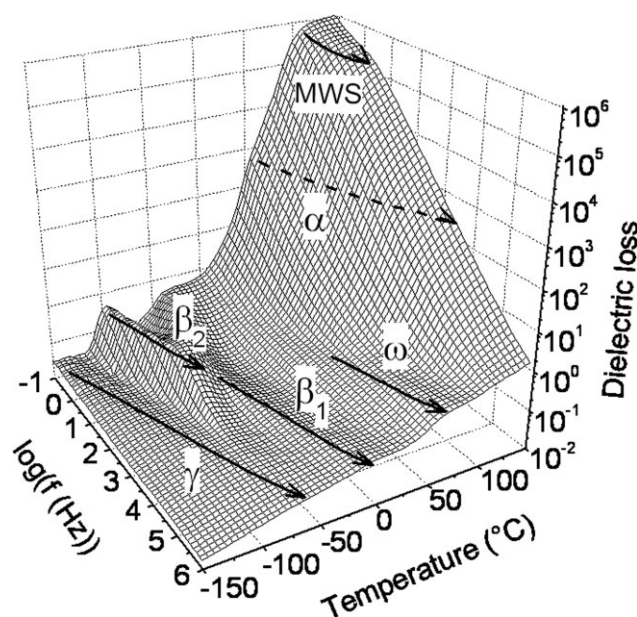


**Figure 5** Dielectric loss at initial state reported on a logarithmic scale as a function of temperature and frequency.

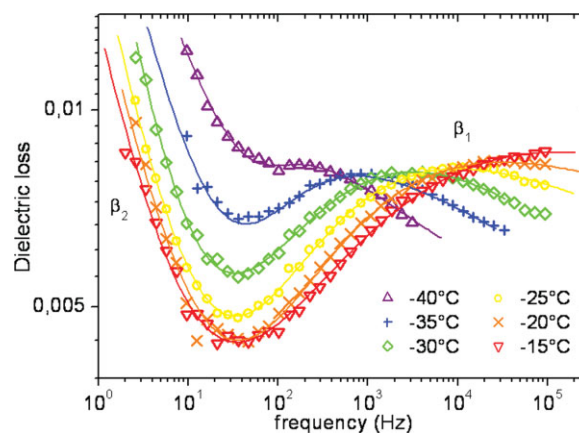


**Figure 6** Isothermal dielectric loss at initial state as a function of frequency showing  $\beta_1$  relaxation. [Color figure can be viewed in the online issue, which is available at [www.interscience.wiley.com](http://www.interscience.wiley.com).]

called  $\beta_1$ . The dielectric loss corresponding to this relaxation is shown in Figure 6 for temperatures ranging from -40 to -15°C. In the high temperature range, three additional relaxations occur:  $\omega$ ,  $\alpha$ , and MWS modes.

Secondary relaxation modes have various molecular origins. The  $\gamma$  mode is related to the  $\text{CH}_2$  mobility in aliphatic chain sequences.<sup>12,13</sup> The molecular origin of  $\beta_2$  and  $\beta_1$  is more complex.  $\beta$  modes are a combination of several molecular entities. According to Ochi et al.,<sup>15</sup>  $\beta$  is mainly associated with the mobility of hydroxyether and diphenyl propane groups. At higher temperatures,  $\omega$  is associated with heterogeneities in the adhesive as observed previously during thermo mechanical measurements.<sup>19</sup>  $\alpha$  is attributed to the dielectric manifestation of glass transition. The MWS relaxation is attributed to macrodipoles.

Relaxation times  $\tau_{\text{HN}}$  are determined using the Havriliak-Negami function [eq. (1)]. The temperature dependence of  $\gamma$ ,  $\beta_2$ , and  $\beta_1$  relaxation times at initial state is reported in the Arrhenius diagram presented in Figure 7. The increase of dynamic dielectric spectroscopy (DDS) measurement temperature shows that  $\gamma$ ,  $\beta_2$ , and  $\beta_1$  modes follow an Arrhenius law as expected [eq. (2)].

$$\tau(T) = \tau_0 \exp\left(\frac{\Delta H}{RT}\right) \quad (2)$$

where  $\Delta H$  is the activation enthalpy,  $\tau_0$  is the pre-exponential factor, and  $R$  is the universal gas constant.

The  $\omega$ ,  $\alpha$ , and MWS evolution is more difficult to analyze. At high temperatures, conductivity appears. Consequently, the use of the HN equation is more complex: we observed a merging between high temperature relaxation modes and conductivity phenomenon. The behavior of these relaxation

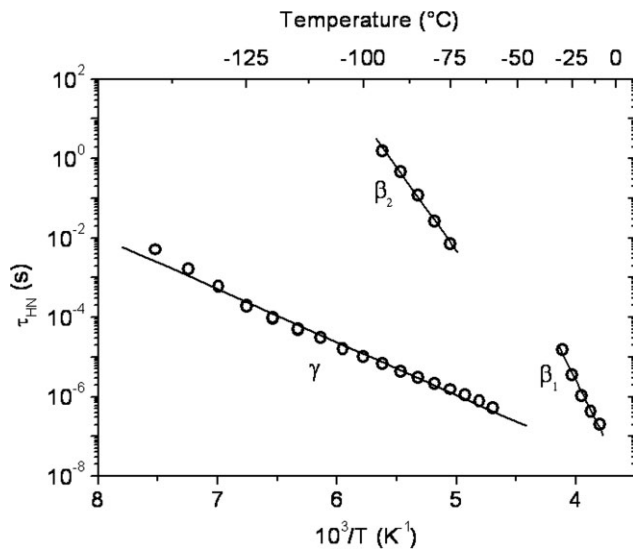


**Figure 7** Relaxation times of  $\gamma$ ,  $\beta_1$ , and  $\beta_2$ : experimental points (o) with Arrhenius fits shown by the solid lines.

phenomena is not presented in this article. We will focus on the evolution of localized mobility associated with secondary relaxation modes as function of hydrothermal aging parameters.

#### Molecular mobility after aging

Hydrothermal aging induces an evolution in  $\gamma$  and  $\beta_1$  behaviors.  $\beta_2$  is not affected. For purpose of clarity, Figure 8 focuses on  $\gamma$  evolution with aging. The higher the aging temperature is, the higher the shift on  $\gamma$ . This change is the same for all moisture content performed at 60 and 80°C.

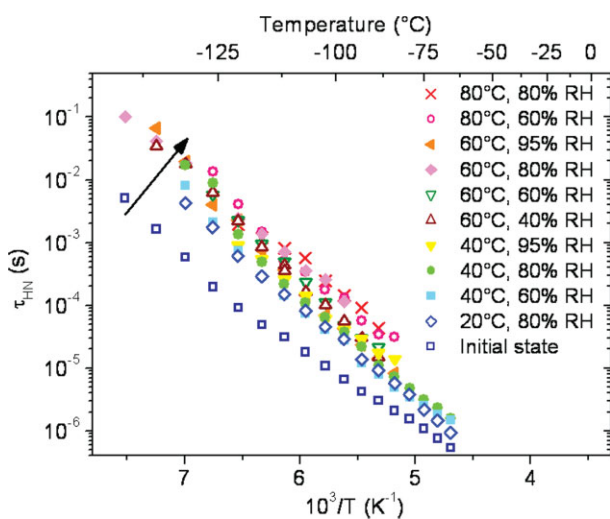


**Figure 8**  $\gamma$  mode relaxation times as a function of temperature after hydrothermal aging. [Color figure can be viewed in the online issue, which is available at [www.interscience.wiley.com](http://www.interscience.wiley.com).]

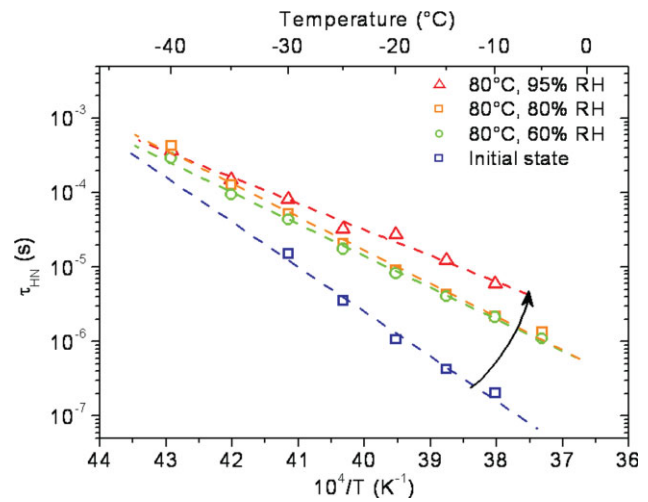


**Figure 9**  $\beta_1$  mode relaxation times after 80°C aging as a function of temperature. [Color figure can be viewed in the online issue, which is available at [www.interscience.wiley.com](http://www.interscience.wiley.com).]

The evolution of  $\beta_1$  relaxation times after hydrothermal aging is presented in Figure 9 after 80°C aging.  $\beta_1$  relaxation times are unchanged in the low temperature range for each case. At 80°C, whatever the relative humidity conditions of the test, i.e. 60–95%RH, the relaxation times associated with  $\beta_1$  are slower than at initial state.

The evolution of  $\beta_1$  relaxation times after 80%RH is presented in Figure 10. At 80%RH, while the DDS temperature measurements increase, the relaxation times shift to higher temperature of 60 and 80°C aging temperatures. After 20 and 40°C aging temperatures, there is no evolution in  $\beta_1$  relaxation times.

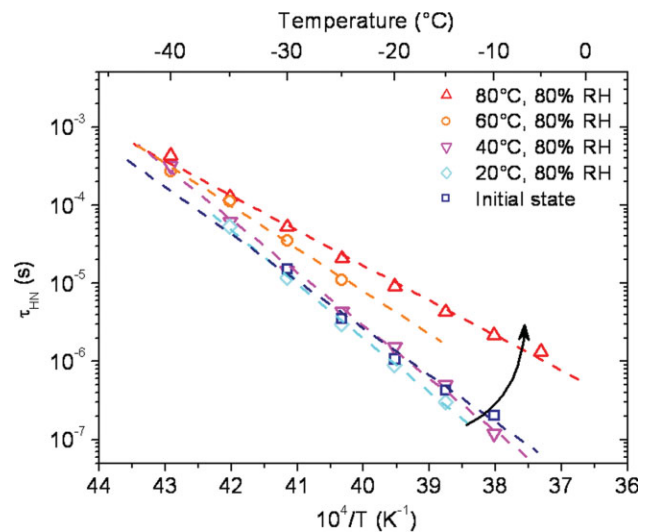


**Figure 10**  $\beta_1$  mode relaxation times after 80% RH aging as a function of temperature. [Color figure can be viewed in the online issue, which is available at [www.interscience.wiley.com](http://www.interscience.wiley.com).]

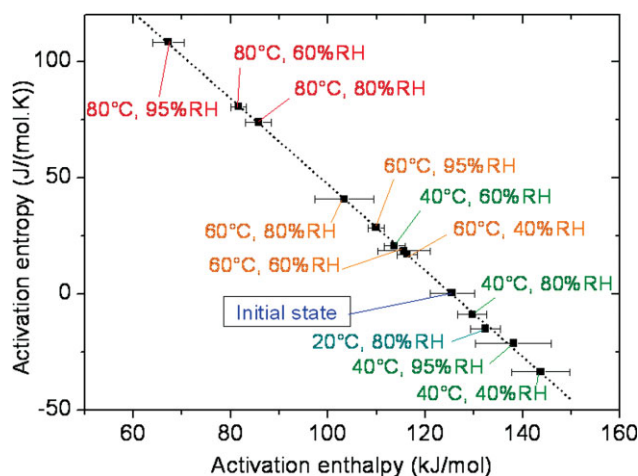


**Figure 11**  $\beta_1$  enthalpy–entropy compensation after hydrothermal aging conditions. [Color figure can be viewed in the online issue, which is available at [www.interscience.wiley.com](http://www.interscience.wiley.com).]

Figures 9 and 10 show a compensation phenomenon at low temperatures. Whatever the aging conditions,  $\tau_{HN}$  is equal to  $10^{-3}$  s at  $-45^\circ\text{C}$ . Similar behavior have already been observed for plasticizers in a polymer matrix.<sup>20</sup>

Activation enthalpy and pre-exponential factors are calculated from eq. (2). According to Eyring theory, eq. (3) gives the activation entropy.

$$\tau_0 = \frac{h}{kT} \exp\left(-\frac{\Delta S}{R}\right) \quad (3)$$

where  $h$  is the Planck constant,  $k$  is the Boltzmann constant, and  $\Delta S$  is the activation entropy.

Activation entropy is reported as function of activation enthalpy on Figure 11. We observe a compensation phenomenon between  $\Delta S$  and  $\Delta H$  for each hydrothermal aging condition. When the aging temperature is 20 and  $40^\circ\text{C}$ , an increase in the activation enthalpy and a decrease in activation entropy compared to initial state was noted. At 60 and  $80^\circ\text{C}$  aging temperatures, the activation enthalpy shifts to lower values while the activation entropy increases.  $\Delta S$  reaches a maximum for the most severe hydrothermal aging parameters.

## DISCUSSION

Figure 2 shows that the temperature aging parameter is preponderant in the mechanical damage induced by hydrothermal tests. When the aging temperature increases, humidity appears more effectively. Such behavior is characteristic of a thermally activated phenomenon like diffusion. Water absorption into the joint is deeply linked to mechanical properties. Failure analysis reported in the Table I shows that

interfacial rupture area increases when the aging conditions are more severe. These results coincide with Cognard approach.<sup>21</sup> Interfacial area could correspond to water clustering between the substrate and the adhesive. The point is emphasized by the slow decrease of the cohesive rupture area and  $\sigma_R$  after 40%RH aging whatever the temperature.

At molecular scale, change in  $\gamma$  behavior with aging is observed on the Figure 8. It is attributed to an annealing effect. Relaxation times associated with  $\gamma$  reach a maximum shift when the test temperature is maximum.  $\Delta H$  is equal before and after aging.  $\tau_0$  increases. This evolution is explained by conformational defaults in aliphatic sequences due to polymerization. In the initial state, some epoxy and amine reactive groups remain into the polymer. They cannot react due to the network cohesion and the limited mobility corresponding to the glassy state.  $\text{CH}_2$  mobility becomes slower with aging temperature. It traduces that conformational state along aliphatic sequences becomes thermodynamically more stable.

Relaxation times corresponding to  $\beta_1$  are shown in Figure 9 and the Figure 10. The evolution of the mobility after aging traduces that around the hydroxyether entities, the physical environment is modified. The influence of aging temperature is pointed out. When the temperature is 60 and  $80^\circ\text{C}$ , whatever the humidity, we observed a decrease in the activation enthalpy and an increase in the activation entropy shown in Figure 11. It means an increase in disorder around hydroxyether moieties. When the aging temperature is  $40^\circ\text{C}$ , the opposite is observed traducing an increase of local order. The temperature treatment influence changes, as function of crossing  $T_\alpha$  shown in Figure 4. Below  $T_g$ , the mobility is limited. Water diffusion is slightly activated. It leads to no evolution at localized scale around the hydroxyether entities. Above the mechanical manifestation of glass transition, the mobility is increased and the diffusion process is more activated due to temperature. The shift in the relaxation times is observed. Some authors observed that  $\beta$  relaxation modes evolve with increasing moisture.<sup>5,8,16</sup> They concluded that hydroxyether (i.e. hydrophilic entity)–water interactions occurs, modifying relaxation times. Though, they observed an increase in hydroxyether mobility when there is an increase in moisture into the joint. In our case, we note that the mobility decreases at high temperature when the hydrothermal aging conditions are more severe. The compensation between entropy and enthalpy also shows the local modification probably due to interaction with water. The loss in molecular mobility traduces this phenomenon. This mode can be used as a dielectrical marker to study hydrothermal effect in adhesive joint.



### Correlation between mechanical and molecular changes

After 7 days of aging in different hydrothermal aging conditions, the studied adhesive exhibits a change in the shear behavior and in the mobility of hydroxyether entities. At macroscopic and molecular scales, we observe that the aging temperature is a more influent parameter than the aging relative humidity percentage. As the aging temperature increases, a decrease in shear rupture stress is denoted. This diminution corresponds to a decrease of hydroxyether mobility in the adhesive. The similarity of these two behaviors let us to think that the water present into the joint bonds with hydroxyether moieties by hydrogen bonds and play a role in diminishing mechanical properties. To complete this study, now we need to analyze the behavior of the  $\alpha$  mode, with hydrothermal aging conditions, i.e. at a delocalised scale in the network. The evolution of the dielectric manifestation of glass transition could confirm the hypothesis that mechanical behavior is linked with the molecular dynamics in this adhesive.

### CONCLUSION

This study points out that the use of dielectric spectroscopy is useful to analyze adhesive bonds. The broad frequency range and the service configuration analyze, i.e. as an adhesive joint, are advantageous. We access the molecular mobility in a configuration similar to classical mechanical tests. The study of hydrothermal effect on bonded assemblies at macroscopic and molecular scales is done. This study allows us to define  $\beta_1$  relaxation mode as a pertinent aging parameter. The shear rupture stress decreases while the relaxation times associated with  $\beta_1$  relaxation mode increases. Their evolutions show that water into the joint is a crucial parameter of hydrothermal aging as expected. It invites to be sure that hydroxyether moieties are linked with  $\beta_1$ , and to study the relationships between water–hydroxyether interactions and mechanical behavior. This result shows that at localized scale, water can act as an aging factor.

The correlation between real aging and accelerated results presented in this article will be completed in a future study. In the same time, real aging influence is analyzed. Mechanical and dielectric behavior are monitored. After 3 years of storage in spacecraft manufacturing conditions, the same parameters, i.e. the relaxation times of  $\beta_1$  and the shear rupture stress, begin to evolve. The study will now focus on the correlation between these different aging conditions.

### References

1. European Cooperation for space Standardization, Thermal testing for the evaluation of space materials, processes, mechanical parts and assemblies, ESA standard document, ECSS-Q-ST-70-04C, 2008.
2. Bellenger, V.; Verdu, J.; Morel, E. *J Mater Sci* 1989, 24, 63.
3. Apicella, A.; Nicolais, L.; De Castaldis, C. *Adv Polym Sci* 1985, 66, 189.
4. Gupta, V. B.; Drzal, L. T.; Lee, C. Y.-C.; Rich, M. J. *Polym Eng Sci* 1985, 25, 812.
5. Mijovic, J.; Zhang, H. *Macromolecules* 2003, 36, 1279.
6. Luo, S.; Leisen, J.; Wong, C. P. *J Appl Polym Sci* 2002, 85, 1.
7. Moy, P.; Karasz, F. E. *Polym Eng Sci* 1980, 20, 315.
8. Colombini, D.; Martinez-Vega, J. J.; Merle, G. *Polymer* 2002, 43, 4479.
9. Nogueira, P.; Ramirez, C.; Torres, A.; Abad, M. J.; Cano, J.; Lopez, J.; Lopez-Bueno, I.; Barral, L. *J Appl Polym Sci* 2001, 80, 71.
10. Comrie, R.; Affrossman, S.; Hayward, D.; Pethrick, R. A. *J Adhes* 2002, 78, 967.
11. Dodiuk, H.; Drori, L.; Miller, J. *J Adhes* 1984, 17, 33.
12. Bershtein, V. A.; Peschanskaya, N. N.; Halary, J. L.; Monnerie, L. *Polymer* 1999, 40, 6687.
13. Boye, J.; Demont, P.; Lacabanne, C. *J Polym Sci Part B: Polym Phys* 1994, 32, 1359.
14. Pangrle, S.; Wu, C. S.; Geil, P. H. *Polym Compos* 1989, 10, 173.
15. Ochi, M.; Kageyama, H.; Shimbo, M. *Polymer* 1988, 29, 320.
16. Maggana, C.; Pissis, P. *J Macromol Sci Phys* 1997, B36, 749.
17. Havriliak, S.; Negami, S. *J Polym Sci Part C: Polym Symp* 1966, 14, 99.
18. Havriliak, S.; Negami, S. *Polymer* 1967, 8, 161.
19. Buch, X. Ph.D. Thesis, Ecole des Mines de Paris, 2000.
20. Hedvig, P. *Dielectric Spectroscopy of Polymers*; Adam Hilger Ltd: Bristol, 1977.
21. Cognard, J. *J Adhes* 1994, 47, 43.